Experimental and theoretical study of Co adsorbed at the surface of Cu: Reconstructions, charge-density waves, surface magnetism, and oxygen adsorption

L. Gonzalez, R. Miranda, M. Salmerón, J. A. Vergés, and Felix Ynduráin
Instituto de Física del Estado Sólido, Consejo Superior de Investigaciones Cientificas, Universidad Autónoma de Madrid, Canto Blanco, Madrid 34, Spain
and Departamento de Física Fundamental, Universidad Autónoma de Madrid, Canto Blanco, Madrid 34, Spain
(Received 22 December 1980)

We have deposited in ultrahigh vacuum Co on top of clean, well-ordered Cu surfaces. The deposition of Co is followed by Auger spectroscopy and by low-energy-electron diffraction. At room temperatures, Co does not diffuse into the substrate: Co grows in two-dimensional islands to form the first layer and from then on the growth is layer by layer. The system Co-Cu(100) shows a $c(2\times2)$ reconstruction when the Cu surface is clean and a $p(2\times2)$ reconstruction when certain impurities are present at the interface. The system Co-Cu(111) shows no reconstruction and the Co grows forming an hcp lattice. The reconstructions of the Co-Cu(100) system are interpreted as being due to ferromagnetic-induced charge-density waves as a detailed electronic-structure calculation reveals. The magnetization and exchange splitting of one layer of Co on top of the Cu(100) surface are very similar to the Co bulk values. We have also studied the adsorption of oxygen in the Co-Cu(100) system for different Co coverages. Our results indicate that as far as oxygen is concerned, the reactivity of Co is not affected by its state of aggregation.

I. INTRODUCTION

In the last decade there has been an important and increasing effort in solid-state research aimed at improving the understanding of the various aspects of single-crystal transition-metal surfaces. Photoemission experiments as well as detailed theoretical calculations have contributed to the knowledge of the electronic structure of some clean transition-metal surfaces.[1] Also the reactivity of single-crystal transition-metal surfaces has been an important subject of research, since it appears as an approach to study catalysis.[2] The electronic configuration of atoms and molecules absorbed at the metal surface,[3] as well as the variation of the reactivity with the presence of defects[4] (steps, kinks, vacancies, etc.) at the metal surface, is by now well characterized.

In order to be closer to the actual structure of a real catalyst, we study in this work the behavior of monolayer and submonolayer reactive transition metal (Co) deposited on top of a single-crystal surface of a nonreactive metal (Cu). This is a partial approach to study the influence of the state of aggregation on the activity of a catalyst. This kind of system is closer to the structure of an actual catalyst than the usually studied single-crystal transition-metal surface, since a real catalyst contains small clusters of a reactive metal deposited on top of an inert substrate (SiO_2, Al_2O_3, etc.).

This work is organized as follows. In Sec. II we describe the experimental procedure to deposit in ultrahigh vacuum, Co on top of Cu. This deposition is controlled by Auger electron spectroscopy (AES), as well as by ultraviolet photoemission (UPS) and low-energy-electron diffraction (LEED). This technique indicates that the presence of Co induces two kinds of reconstructions [$c(2\times2)$ or $p(2\times2)$] in the system for the (100) surface orientation of Cu and none for the (111) surface orientation. In Sec. III, we develop a theoretical model for the electronic structure of the Co-Cu system. Both the $c(2\times2)$ and $p(2\times2)$ reconstructions of the Co-Cu(100) system are predicted by our model. These reconstructions are interpreted as being due to ferromagnetic induced charge-density waves (CDW's). In Sec. IV, we study the adsorption of oxygen on the Co-Cu(100) system. We study the dependence of the O_2 adsorption with the thickness of the Co overlayer, varying from less than one monolayer to several (~10) layers. Finally, in Sec. IV, some final remarks and conclusions are made.

II. EXPERIMENTAL CHARACTERIZATION OF THE Co-Cu SYSTEM

All measurements were performed in a UHV system equipped with a four-grid LEED optics, a single-pass cylindrical mirror analyzer (CMA) for AES, a light source for UPS, and the usual facilities for cleaning the sample and controlling the residual gas composition. The base pressure was in the low 10^{-10} Torr range, increasing to 8×10^{-10} Torr when performing UPS measurements due to the helium leaking into the chamber. The light source for the UPS studies was a Vacuum Generator windowless discharge lamp. Photoemission spectra were obtained with the same single-pass CMA used for Auger spectroscopy. There are some problems with this way of taking the UPS spectra. The absence of retardation makes the

energy window, ΔE, decrease linearly with the electron energy. This is responsible for the absence of the low-energy secondary electron tail in our spectra (see below).

The Cu surfaces were cleaned by Ar^+ bombardment (600 eV, 2 $\mu A/cm^2$, 10 min) and ordered by annealing (800 K, 30 min). The most common impurities present were C and S, which could be easily reduced below the limit of detection (0.005 monolayers). The evaporation of Co was done by heating a small Co wire in front of the Cu crystal. The evaporation rate was kept constant and the deposition dose was carefully controlled by opening, for fixed periods of time, a shutter which screens the Co filament source. In this way we have grown,[5] in ultrahigh vacuum, Co on top of two different clean, well ordered Cu surfaces [the Cu(100) and Cu(111)]. The deposition of Co has been followed by AES, LEED, and UPS. For both Cu-surface orientations, the Co Auger peaks are very stable, indicating negligible dissolution at room temperature of Co into the Cu substrate. Dissolution begins to take place at about 600 K. We now discuss the two Cu-surface orientations studied separately.

(i) Co-Cu(100). In Fig. 1 we show the evolution of the peak-to-peak intensities of the $M_I M_{45} M_{45}$ (95 eV) and the $L_{111} M_{23} M_{45}$ (716 eV) Auger transitions of Co and the $M_I M_{45} M_{45}$ (105 eV) Auger transition of Cu as a function of the Co evaporation doses. Also, the observed LEED patterns are shown in this figure. The linear variation of the Auger peak intensities for both the substrate and the adsorbate indicates a two-dimensional layer-by-layer growth of Co. The breaks in the otherwise linear behavior occur at the same Co evapor-

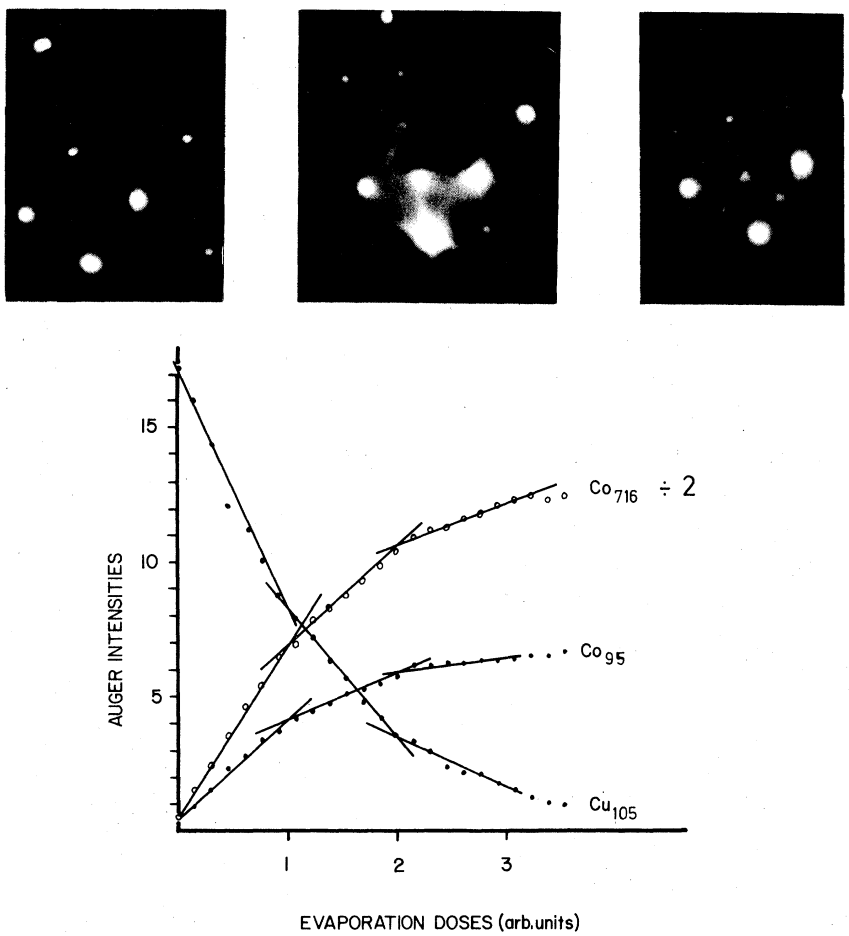

FIG. 1. Peak-to-peak intensities (×100) of Cu $M_I M_{45} M_{45}$ (105 eV) Auger transition and Co $M_I M_{45} M_{45}$ (95 eV) and $L_{III} M_{23} M_{45}$ (716 eV) Auger transitions versus Co evaporation doses on Cu(100) surface. Intensities are normalized to the initial value of the $L_{111} M_{45} M_{45}$ (920 eV) Auger transition of Cu. In the upper half of the figure, from left to right, LEED patterns (at 120 eV) correspond to clean Cu(100), one monolayer of clean cobalt and one monolayer of cobalt on a sulfur-contaminated Cu surface.

ation doses for both Co and Cu Auger peaks. Since each break takes place after the same amount of Co deposited, they indicate the completion of the different Co layers, the first Co monolayer then being reached at the first break. Also in Fig. 1, we show the observed LEED patterns. Before any Co evaporation, we observe the familiar (1×1) pattern, corresponding to a clean, ordered Cu(100) surface. After deposition of approximately one-third of a Co monolayer, a stable $c(2\times2)$ reconstruction is observed which persists when several Co layers are deposited. Finally, also in Fig. 1 we show the LEED pattern corresponding to a $p(2\times2)$ reconstruction of the Co-Cu(100) system which is stabilized by the presence of one-third of a sulfur monolayer near the surface. The $p(2\times2)$ LEED pattern was never observed when the surface was clean.

(ii) Co-Cu(111). We have followed the same procedure described above for the evaporation of Co on a clean Cu(111) surface. In Fig. 2, we show the evolution of the peak-to-peak intensities of the Auger transitions of both Cu and Co. These curves have been obtained using the four-grid LEED optics as a retarding field analyzer for the Auger electrons; therefore the intensities cannot be directly compared with those in Fig. 1. The steep background level on which these reported peak-to-peak intensities are superimposed has not been subtracted. The results shown in Fig. 2 indicate that Co on top of Cu(111) behaves like Co on top of a Cu(100) surface. The LEED pattern also shown in Fig. 2 indicates that deposition of Co on top of a Cu(111) surface does not induce any reconstruction. The analysis of the variation of the LEED patterns (see Fig. 2) upon adsorption of Co reveals a change from a threefold symmetry in a clean Cu surface to a sixfold symmetry when Co is deposited up to ~8 layers. This seems to indicate that Co grows on top of Cu(111) in the hcp structure rather than in the fcc one.

From the above reported experimental results we can conclude the following. (a) Co does not diffuse into Cu at room temperature. We can heat the system up to 600 K until appreciable dissolution of Co occurs. (b) Co deposited on top of a clean Cu(100) surface gives rise to a $c(2\times2)$ reconstruction. (c) The fact that the stable $c(2\times2)$ LEED pattern in the Co-Cu(100) system is observed from approximately one-third of a Co

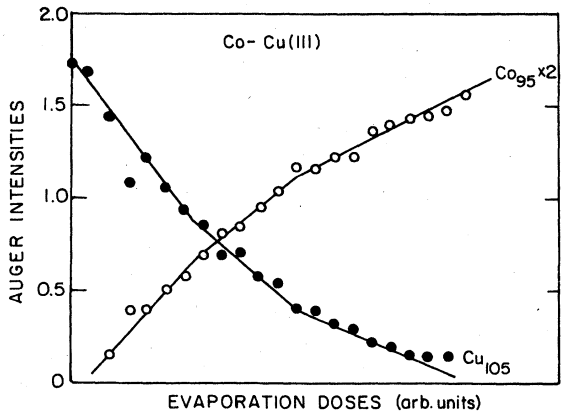

FIG. 2. Peak-to-peak intensities of Cu and Co Auger transitions as a function of Co evaporation doses on top of Cu(111) surface. Intensities are referred to clean-Cu 920-eV Auger peak. LEED patterns, in the upper part of the figure, correspond, from left to right, to a clean Cu(111) surface and to one monolayer of cobalt deposited on it.

monolayer indicates that Co forms two-dimensional islands that grow to form a full monolayer. From then on, the growth of Co is layer by layer as the evolution of Auger peaks shows. (d) No reconstruction takes place on the Cu(111) surface upon adsorption of Co. (e) On the Cu(111) face, Co grows also layer by layer and, after several layers, shows the sixfold symmetry, characteristic of the hcp system.

III. THEORETICAL MODEL

In order to elucidate which mechanism is responsible for the above-discussed reconstructions, we have performed a detailed electronic-structure calculation of the Co-Cu system in the case of one monolayer of Co.

The calculation has been performed using a realistic tight-binding Hamiltonian, which includes five d orbitals, three p orbitals, and one s orbital per atom and interactions between orbitals in first- and second-nearest-neighbor atoms. The interaction parameters for Cu have been fitted to reproduce Burdick's bulk band-structure calculation.[6] They also give a good description[7] of the Cu electronic surface structure. The Hamiltonian parameters for Co–Cu and Co–Co bonds have been taken to be like those of the Cu–Cu bond, the difference between Co and Cu being then the energy of the atomic orbitals.

To calculate the density of states of the Co-Cu system, we first assume that the Co atoms at the Co layer are at the hollow positions on top of the Cu surface, such that the Co–Cu bond length is identical to the Cu–Cu bond length. Once the structure and the Hamiltonian are fixed, we calculate the local density of states at the various layers of the system. The density of states is calculated using the transfer matrix method.[8] In this method, the atomic wave functions in a layer form a Bloch function with well defined k_{11} (wave vector parallel to the surface). In this basis, the problem is reduced to a one-dimensional one for each k_{11}. This one-dimensional problem is solved in real space using the transfer matrix technique, which gives the Green's function, and from its imaginary part the density of states is obtained. Once the density of states is obtained for each k_{11}, integration over the two-dimensional Brillouin zone gives the density of states.

Results of our calculations for paramagnetic Co in the Co-Cu(100) and Co-Cu(111) systems are drawn in Figs. 3 and 4, respectively. The relative positions of the Co atomic orbital energies with respect to those of Cu are fixed by requiring local charge neutrality everywhere. The density of states for the Co-Cu(100) and Co-Cu(111) surfaces were obtained by sampling ten and six representative points[9] in the two-dimensional Brillouin zone, respectively. In both Figs. 3 and 4, we see that the d bands of Cu and Co are ~3 eV apart; in other words, the interaction between the d orbitals in the Cu substrate and the Co overlayer is rather weak. This is due to the fact that the d orbital energy of Co is 3 eV higher than the corresponding energy of Cu, as local charge neutrality requires. In Fig. 3, we have also drawn the density of states at a free Cu(100) surface. We see immediately in this figure that the effect of the Co layer on the Cu d states is rather weak. In fact the density of d states at the Co layer in the systems Co-Cu(100) and Co-Cu(111) is very similar to a two-

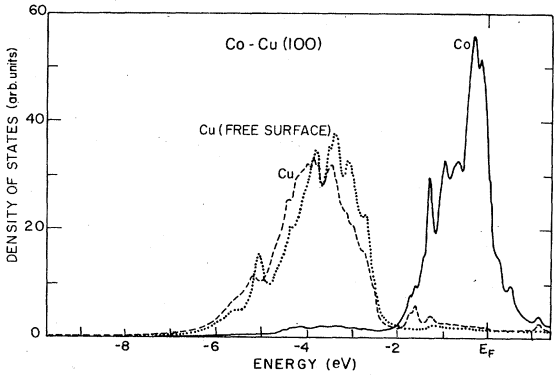

FIG. 3. Electronic density of states for one unreconstructed paramagnetic monolayer of Co on top of a Cu(100) surface. The heavy line represents the local density of states at the Co layer, the broken line corresponds to the density of states at the underneath Cu layer and the dotted line represents the density of states of a Cu(100) free surface. The energies are referred to the Fermi level and all the curves are normalized to nine states per atom.

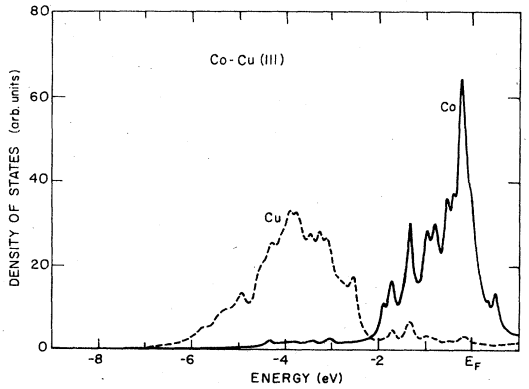

FIG. 4. Electronic density of states for one paramagnetic monolayer of Co deposited on top of a clean Cu(111) surface. The heavy line represents the local density of states at the Co layer and the broken line represents the density of states at the underneath Cu layer.

dimensional single layer of Co.

In order to see if our calculation gives a good description of the Co-Cu system, we have performed an ultraviolet photoemission measurement (the resolution in energy at the Fermi level being $\Delta E \simeq 0.3$ eV) of the Co-Cu(100) system for various Co coverages. Our experimental results, along with the calculated densities of states, are drawn in Fig. 5. We see that there is a fairly good agreement between theory and experiment. Both give an important Co-associated increase of states near the Fermi level. The difference spectrum between $\theta = 1$ and 0, Fig. 5(b), indicates that the energy difference between the d bands of Cu and Co is about 2 eV. The discrepancy between theory and experiments near E_F might be due to the fact that the calculation is for a paramagnetic unreconstructed Co overlayer (see below).

From the experimental results discussed above and in the preceding section, we can conclude that one layer of Co in the Co-Cu system behaves essentially like a two-dimensional transition metal. In a system like this, CDW instabilities are likely to take place as in layer compounds.

In order to investigate whether the reconstructions found in the Co-Cu(100) system are due to a CDW, we have first calculated the electronic states of a two-dimensional simple cubic lattice of Co for the Hamiltonian described above. Constant-energy contours for the bands with dominant d character are drawn in Fig. 6. In this figure, we notice that if the Fermi level were near the constant-energy contour label 9, we would get a nesting[10] of the Fermi line [see Fig. 6(c)] and then a CDW compatible with the $p(2\times 2)$ reconstruction. On the other hand, we see in Fig. 6(d) that the nesting of the Fermi line would give rise to a $c(2\times 2)$ reconstruction. Also pockets of electrons between the points Γ and K of the Brillouin zone [see Fig. 6(e)] would give rise to CDW's (Ref. 11) compatible with both the $p(2\times 2)$ and the $c(2\times 2)$ reconstructions.

The existence of dispersionless constant-energy contours may be due to the strict two-dimensionality of our calculation. In order to see whether this is so, we have analyzed the full Co-Cu(100) system. In this case, we cannot draw constant-

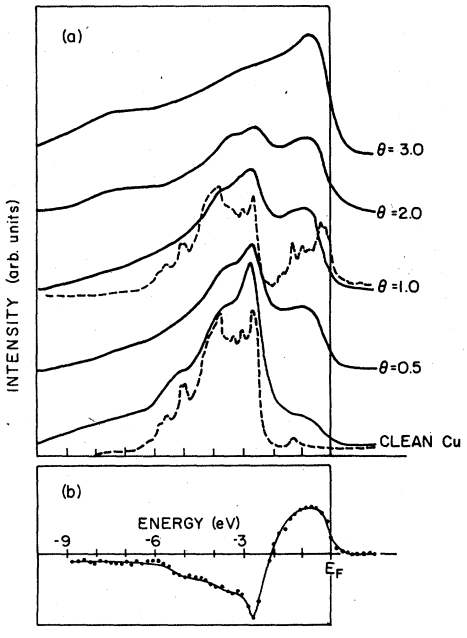

FIG. 5. (a) Heavy lines: ultraviolet photoemission spectra ($h\nu = 21.2$ eV) of the Co-Cu(100) system for different Co coverages (indicated by θ). Dotted line: theoretical calculation of the electronic density of states. (b) Difference spectrum ($\times 1$) between the spectrum corresponding to one monolayer of Co ($\theta = 1$) and that corresponding to the clean Cu(100) surface.

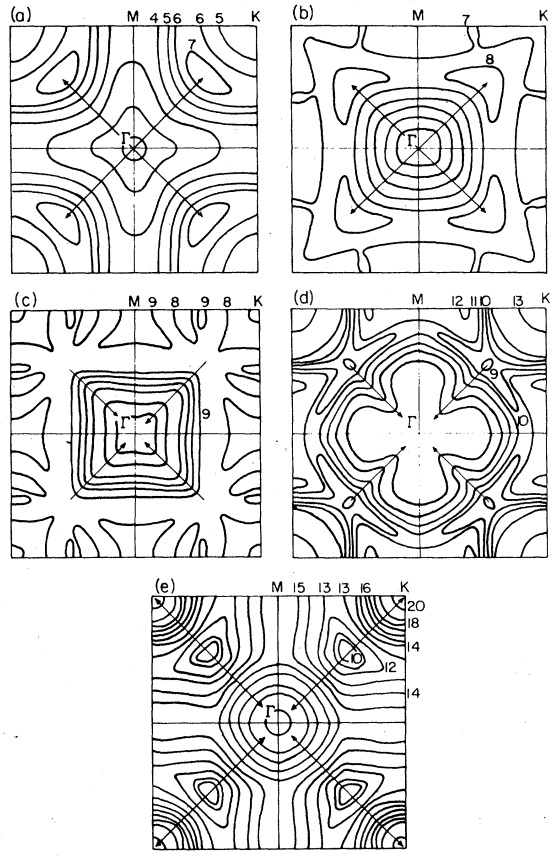

FIG. 6. Contours of constant energy for the five d bands of Co in a two-dimensional simple square lattice. The arrows indicate increasing energies. The energy difference between two adjacent constant-energy contours is 0.07 eV except in the two top panels where it is 0.14 eV.

energy contours since the d levels of Co hybridize with the s-p bands of Cu (see Fig. 3). We have calculated then the Co-layer local density of states along several directions in the two-dimensional Brillouin zone. Results of our calculations are drawn in Fig. 7.

In Fig. 7(a), we show the densities of states along the line M–H in the Brillouin zone. We observe a peak in the density of states at ~0.4 eV below the paramagnetic Fermi level (origin of energies in the figure), whose position is independent of k_{11}. This is related indeed to the dispersionless constant-energy contour in Fig. 6(d). On the other hand, we observe in Fig. 7(b) a peak in the density of states at ~−0.6 eV, whose position does not change along the line H–F: It is related to the dispersionless constant-energy contour in Fig. 6(c). We believe that this behavior is independent of the Hamiltonian and is due to the symmetry of the problem. If we consider the Co orbital d_{xy} (z being the normal to the surface) it can be seen that the only intralayer d-d interaction allowed by symmetry is the d_{xy}-d_{xy} interaction, which would give the following dispersion relation if hybridization is neglected,

$$E = 2V_{xy}(\cos k_x \pi/a + \cos k_y \pi/a)\,, \tag{1}$$

where V_{xy} is the nearest-neighbor d_{xy}-d_{xy} interaction and a is the lattice constant. Equation (1) gives a dispersionless band along the line M–M as in Figs. 6(d) and 7(a).

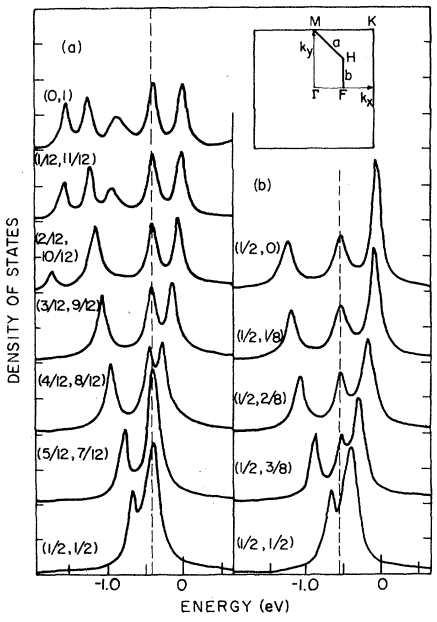

FIG. 7. Densities of state at the Co layer for the unreconstructed paramagnetic Co-Cu(100) system for different k points in the two-dimensional Brillouin zone. (a) Density-of-state curves along MH. (b) Density of state curves along HF. The energy scale is as in Fig. 3.

On the other hand, it can easily be seen that Co d_{xz} and d_{yz} orbitals give rise to essentially one-dimensional bands along k_x and k_y, respectively, then being responsible for the dispersionless bands in Figs. 6(c) and 7(b).

As we can see in Fig. 7, the "dispersionless peaks" are 0.4 and 0.6 eV below the paramagnetic Fermi level, respectively. If Co is paramagnetic, these peaks are too far from the Fermi level to give rise to a Peierls distortion. In our calculation, there are two electrons per Co atom between 0 and −0.4 eV; then although it is difficult to fix the position of the Fermi level very accurately, we believe that if Co is paramagnetic, by no means can the Fermi level be at the energy of the "dispersionless peaks."

So far we have assumed that Co is paramagnetic. The Stoner condition for ferromagnetism is

$$U\rho(E_F) \geq 1 \tag{2}$$

where U is the Hubbard[12] electron-electron interaction and $\rho(E_F)$ is the paramagnetic density of states at the Fermi level.

Condition (2) is satisfied for both the Co-Cu(100) and Co-Cu(111) systems, since $\rho(E_F)$ is approximately 2.5 states/eV and U is of the order of 1 eV. We then expect Co to be ferromagnetic in the Co-Cu system. Anomalous Hall-effect measurements[13] indicate that a monolayer of Co absorbed on a nonmagnetic amorphous substrate is ferromagnetic at low temperatures.

We have taken then Co to be ferromagnetic, with the same magnetization[14] as bulk Co ($n\uparrow = 5.28$ and $n\downarrow = 3.72$) and assume a rigid-exchange-band approximation. In this case, the minority-spin Fermi level lies at ~0.4 eV below the paramagnetic Fermi level where the "dispersionless peak" compatible with the $c(2\times 2)$ reconstruction appears [see Fig. 7(a)]. This result is also in agreement with directional photoemission data[15] for bulk Co, which give an exchange splitting in the range 0.8–1.1 eV. Our calculation indicates than that the $c(2\times 2)$ reconstruction in the Co-Cu(100) system is a ferromagnetic induced charge-density wave. The model is also consistent with the experimental result concerning the $p(2\times 2)$ reconstruction of the Co-Cu(100) system. Electron-acceptor impurities, such as S, can lower the Fermi level to meet the nesting condition compatible with the $p(2\times 2)$ reconstruction, i.e., the "dispersionless peak" in Fig. 7(b).

It should be pointed out that we have also made the same analysis for the Co-Cu(111) system. We have found no dispersionless constant-energy contours in agreement with our experimental results

indicating no reconstruction of this surface.

The coexistence of ferromagnetism and CDW's has been discussed by Balseiro *et al.*[16] They have solved a Hamiltonian of the form

$$H=\sum_k E_k C_k^\dagger C_k+\sum_q \hbar\omega_q b_q^\dagger b_q+U\sum_i n_{i\uparrow} n_{i\downarrow}$$

$$+\frac{1}{\sqrt{N}}\sum_k\sum_q g(q)C_{k+q}^\dagger C_k(b_q+b_{-q}^\dagger)\,, \qquad (3)$$

where E_k is given by (1), $C_k^\dagger$ (C_k) is the electron creation (annihilation) operator, $b_q^\dagger$ (b_q) is the phonon creation (annihilation) operator, $g(q)$ is the electron-phonon interaction, and the second term of (3) gives the elastic energy. The Hartree-Fock solution of (3) gives the phase diagram[15] of Fig. 8. This result indicates the possibility of the coexistence of ferromagnetism and CDW's. The results of Ref. 16 indicate that the important condition to get the CDW instability is the existence of constant-energy contours, the position of the Fermi level being less important since ferromagnetism repopulates the spin subbands such that one of them meets the nesting condition lowering the energy of the system.

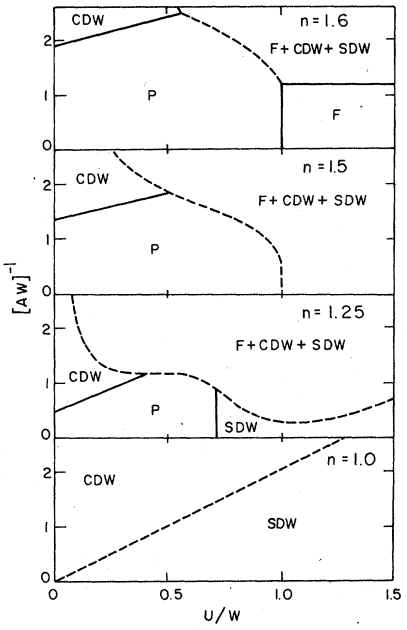

FIG. 8. Phase diagram (see Ref. 16) for different occupation numbers n. W is the bandwidth and A is proportional to the elastic energy divided by the electron-phonon matrix element squared. In general, for $n > 1$ the CDW and the magnetic order interface in a constructive way (see reference for details).

IV. THE ADSORPTION OF OXYGEN IN THE Co-Cu(100) SYSTEM

In order to study the reactivity of the reconstructed layer of Co and the influence of the state of aggregation in the chemical reactivity of Co, we have studied the adsorption of a simple molecule such as O_2 on the clean Cu(100) surface, and on Cu(100) surfaces with submonolayer and monolayer amounts of Co deposited.

The oxygen was admitted into the chamber through a leak valve and the exposure was calculated from the corrected ion-gauge reading. The intensity of the oxygen *KLL* Auger transition at 512 eV was recorded as a function of the oxygen exposure. Results for various Co coverages (given

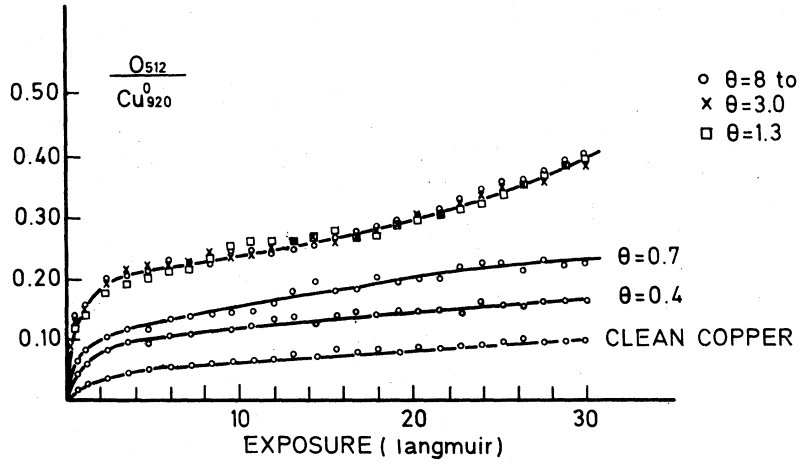

FIG. 9. Peak-to-peak intensity of the oxygen KLL Auger transition versus oxygen exposure for different Co coverages on the Co-Cu(100) system. The intensities are normalized to the initial clean Cu_{920} peak value. The oxygen partial pressure is 2×10^{-8} Torr and the exposure is given in langmuirs ($1\ L=10^{-6}$ Torr sec).

by θ) and for clean Cu(100) are shown in Fig. 9. It should be noted that the oxygen peak intensities are normalized to the initial value of the intensity of the Cu $L_{111}M_{45}M_{45}$ (920 eV) Auger transition.

The adsorption of oxygen on clean Cu(100) proceeds slowly with an initial sticking coefficient $s_0 \simeq 0.04$. This value is in good agreement with previous results obtained by other groups.[17] The oxygen adsorption gives rise to a $c(2\times2)$ LEED pattern for oxygen exposures much higher than that shown in the figure. The saturation value of O_{512}/Cu_{920} is 0.22, which should correspond to 0.5 monolayer of oxygen if the $c(2\times2)$ structure covers the whole surface.

We will discuss separately the Co submonolayer regime and the multilayer regime.

(i) Several Co monolayers ($\theta > 1$). For Co coverages greater than one monolayer ($\theta = 1$), we first notice that the oxygen adsorption does not depend on the Co coverages. In fact, the curves for $\theta = 1.3$, 3.0, and 8 monolayers can be superimposed. Also, the oxygen adsorption on the reconstructed monolayer of Co on top of Cu(100) behaves essentially like the oxygen adsorption on the two single-crystal Co surfaces that have been studied [Co(0001) (Ref. 18) and Co(100) (Ref. 19)].

The chemisorption of oxygen takes place in these surfaces with high initial sticking coefficient ($s_0 \simeq 0.8$). The adsorption curve in Fig. 9 increases rapidly up to a value of $O_{512}/Cu_{920} = 0.22$ for approximately 4 langmuirs. This is followed by a plateau extending up to about 12 langmuirs, which corresponds to the formation of the chemisorbed layer.

The LEED pattern does not change during the chemisorption process; it remains $c(2\times2)$ as in the clean reconstructed Co monolayer. So far, no I-V profiles have been measured. Therefore nothing can be said about the atomic structure of both $c(2\times2)$ reconstructed surfaces. The oxygen-induced $c(2\times2)$ LEED pattern has also been observed on Co(100).[20]

The chemisorption stage is followed by the nucleation and growth of a surface oxide layer which corresponds to the slow increase in the oxygen signal that can be seen in Fig. 9, from approximately 12 langmuirs. The initial oxidation stage is very similar for different Co coverages. The saturation values for complete oxidation depend on the thickness of the Co film, as can be seen in Fig. 10. The saturation values for $\theta \sim 8$–10 are already similar to those of single-crystal Co surfaces.[18,19] They correspond to a "surface oxide" between two and three layers in width, as has also been observed in Ni(100).[21] The lower saturation value rached for $\theta = 1.3$ corresponds to 1.3 monolayers of stoichiometric CoO, as can be easily deduced from our data.

(ii) Submonolayer regime ($\theta > 1$). In the Co sub-

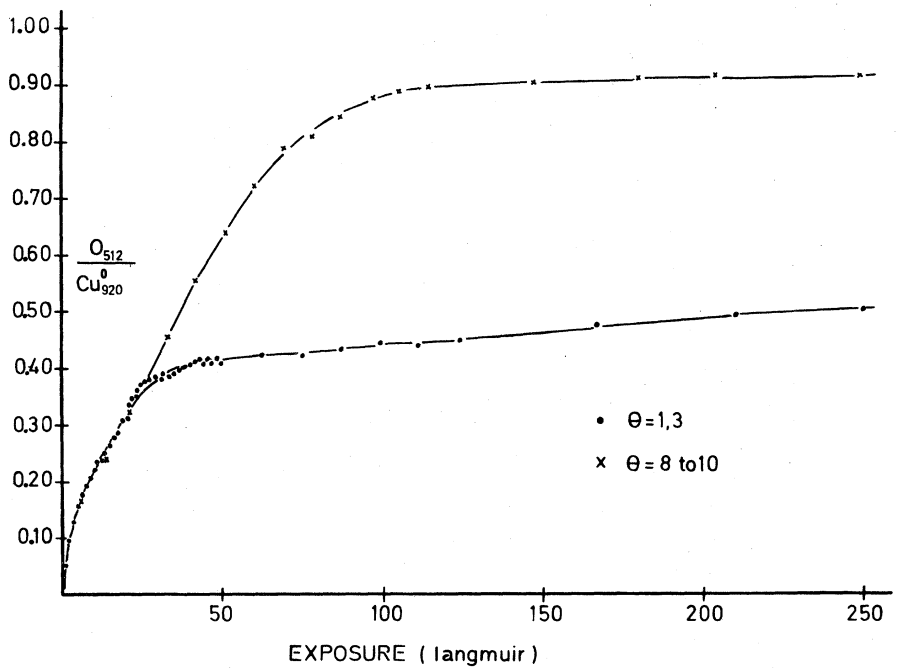

FIG. 10. Intensity of the oxygen *KLL* Auger peak referred to the intensity of the initial Cu_{920} peak as a function of oxygen exposure. The oxygen partial pressure is 1×10^{-7} Torr.

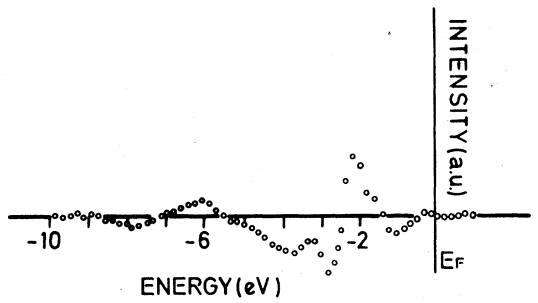

FIG. 11. Ultraviolet difference photoemission spectrum ($h\nu = 21.2$ eV) for 6 L of oxygen chemisorbed on a submonolayer ($\theta = 0.4$) cobalt-covered surface.

monolayer regime ($\theta < 1$), the initial stage (see Fig. 9) is different from that observed for $\theta > 1$. Here the overall uptake of oxygen proceeds at a slower rate. It saturates at oxygen exposures exceeding the range shown in Fig. 9. The final value of the ratio O_{512}/Cu_{920} is 0.22, independent of the value of θ provided this is less than 1.

The observed behavior, e.g., the initial sticking coefficient, for a given Co coverage can be easily explained as a linear combination of the curves corresponding to $\theta = 0$ and 1, with coefficients equal to the fraction of Co and Cu exposed surfaces. The system can be thought of as composed of a certain part of the surface covered by Co islands, the rest of the surface being clean Cu. The oxygen adsorption takes place on the Co islands with the same kinetic characteristics as in a full monolayer of Co.

Ultraviolet photoemission studies have also been carried out for the oxygen chemisorption on different Co layer thicknesses, looking for changes in the oxygen–cobalt bonding. The results, in the form of a difference spectrum for 6 langmuirs of oxygen chemisorbed on the surface covered with $\theta = 0.4$ monolayers, are drawn in Fig. 11. The spectrum shows two peaks at 2 and 6 eV below the Fermi level, which are common to the oxygen adsorption in a number of chemisorbed and oxidized metals.[22] We see no relevant changes in the binding when going from below the cobalt monolayer to various layers.

We can thus conclude that, as far as the interaction with oxygen is concerned, there are no significant differences in the chemical reactivity when changing the state of aggregation of cobalt. This indicates that the interaction between cobalt and oxygen is basically an atomic process. The adsorption characteristics of oxygen in this system, i.e., initial sticking coefficient, chemisorbed layer and subsequent oxide formation, bonding to the Co, etc., can be explained on the basis of the known behavior of Co(100) and Cu(100) cyrstals.

V. CONCLUDING REMARKS

The work we have discussed above can be summarized in the following points.

(i) Co does not diffuse into Cu at room temperature. This gives rise to an essentially two-dimensional transition metal where instabilities are likely to take place. The Co-Cu system is rather unique since other transition metals diffuse into bulk Cu at room temperature.

(ii) Cobalt grows on top of Cu, forming two-dimensional islands until the completion of the first monolayer. From then on, the growth of Co is layer by layer.

(iii) The Co-Cu(100) system shows a $c(2\times2)$ reconstruction upon adsorption of a fraction of a Co monolayer and persists when several layers of Co are deposited. The Co-Cu(111) system shows no reconstruction, the Co growing to form an hcp structure.

(iv) Ultraviolet photoemission spectra taken for various Co coverages in the Co-Cu(100) system, are in good agreement with calculated densities of states for the same system. These results indicate that the interaction between the d orbitals of Co and Cu is rather weak.

(v) The Stoner condition for ferromagnetism is satisfied in both Co-Cu(100) and Co-Cu(111) systems, indicating that a single layer of Co can be ferromagnetic in agreement with anomalous Hall-effect measurements.[13]

(vi) A detailed calculation of the electronic structure of the Co-Cu(100) system indicates the existence of a nesting of the minority-spin Fermi surface which indicates that the $c(2\times2)$ reconstruction of the Co-Cu(100) system is due to a ferromagnetic-induced charge-density wave.

(vii) Our study of adsorption of O_2 in the Co-Cu(100) system indicates that the reactivity of Co is scarcely affected by its state of aggregation as far as oxygen is concerned.

ACKNOWLEDGMENT

The work at the Departamento de Física Fundamental was supported in part by the U. S.-Spain Friendship and Cooperative Treaty, Complementary Agreement No. 3.

[1]See, for instance, S. Hüfner, in *Photoemission in Solids II*, edited by M. Cardona and L. Ley (Springer, Berlin, 1978), p. 192.
[2]J. J. McCarroll, Surf. Sci. 53, 297 (1975); H. P. Bonzel, *ibid.* 68, 236 (1977).
[3]See, for instance, B. Feuerbacher and B. Fitton, in *Electron Spectroscopy for Surface Analysis*, edited by H. Ibach (Springer, Berlin, 1977), pp. 151–197, and references therein.
[4]G. Somorjai, Surf. Sci. 89, 496 (1979).
[5]S. Ferrer, L. Gonzalez, M. Salmerón, J. A. Vergés, and Felix Yndurain, unpublished.
[6]G. A. Burdick, Phys. Rev. 129, 138 (1963).
[7]J. A. Vergés and F. Yndurain, Solid State Commun. 29, 635 (1979).
[8]F. Yndurain and L. M. Falicov, Phys. Rev. Lett. 37, 928 (1976).
[9]S. L. Cunningham, Phys. Rev. B 10, 4988 (1974).
[10]See, for instance, J. A. Wilson, F. J. DiSalvo, and S. Mahajan, Adv. Phys. 24, 117 (1975).
[11]M. J. Kelly and L. M. Falicov, Phys. Rev. B 15, 1983 (1977).
[12]J. Hubbard, Proc. R. Soc. London A276, 238 (1963); A277, 237 (1964); A281, 401 (1964).
[13]G. Bergmann, Phys. Rev. Lett. 41, 264 (1978).
[14]F. Batallán, I. Rosenman, and C. B. Sommers, Phys. Rev. B 11, 545 (1975).
[15]F. J. Himpsel and D. E. Eastman, Phys. Rev. B 21, 3207 (1980).
[16]C. A. Balseiro, P. Schlottmann, and Felix Yndurain, Phys. Rev. B 21, 5267 (1980).
[17]There are many papers on the adsorption of O_2 on Cu(100); see, for instance, P. Hoffmann, R. Unwin, W. Wyrobisch, and A. M. Bradshaw, Surf. Sci. 72, 635 (1978).
[18]M. E. Bridge and R. M. Lambert, Surf. Sci. 82, 413 (1979).
[19]G. Rovida and M. Maglietta, in *Proceedings of the 7th International Vacuum Congress and 3rd International Conference on Solid Surfaces* (IVC, ICSS, Vienna, 1977), p. 963.
[20]M. Maglietta, E. Zanazzi, U. Bardi, and F. Jona, Surf. Sci. 77, 101 (1978).
[21]R. Miranda, M. Salmerón, and J. M. Rojo, Solid State Commun. 35, 83 (1980).
[22]J. Küppers and G. Ertl, Surf. Sci. 77, L647 (1978).

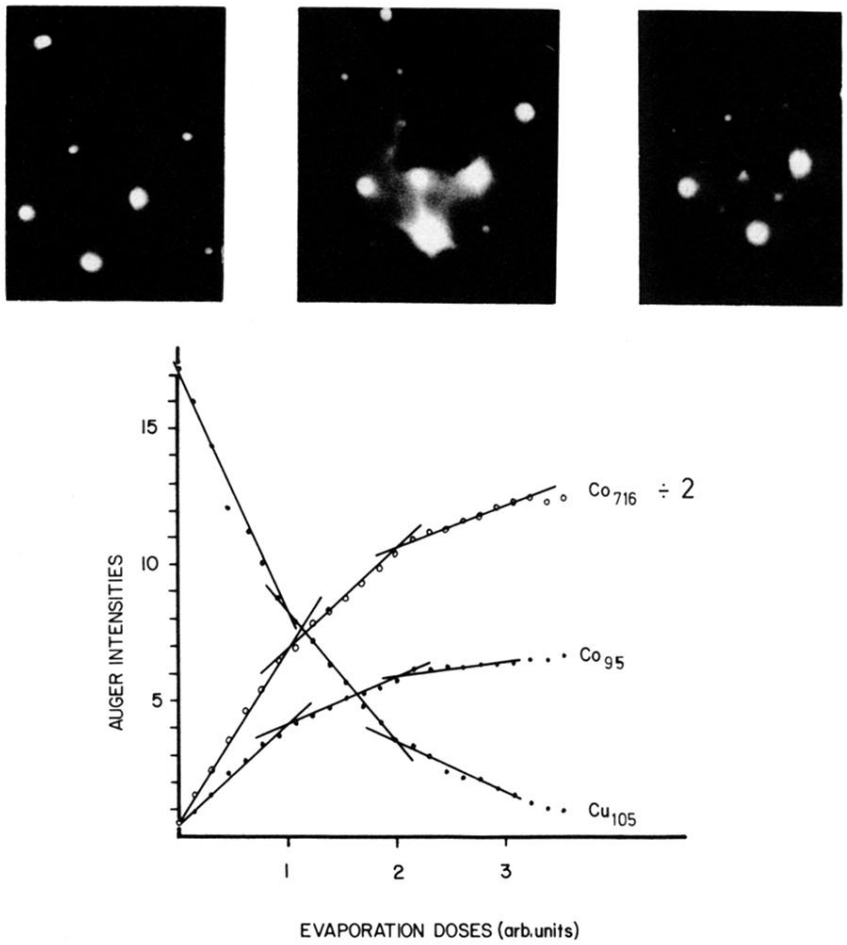

FIG. 1. Peak-to-peak intensities (×100) of Cu $M_I M_{45} M_{45}$ (105 eV) Auger transition and Co $M_I M_{45} M_{45}$ (95 eV) and $L_{III} M_{23} M_{45}$ (716 eV) Auger transitions versus Co evaporation doses on Cu(100) surface. Intensities are normalized to the initial value of the $L_{111} M_{45} M_{45}$ (920 eV) Auger transition of Cu. In the upper half of the figure, from left to right, LEED patterns (at 120 eV) correspond to clean Cu(100), one monolayer of clean cobalt and one monolayer of cobalt on a sulfur-contaminated Cu surface.

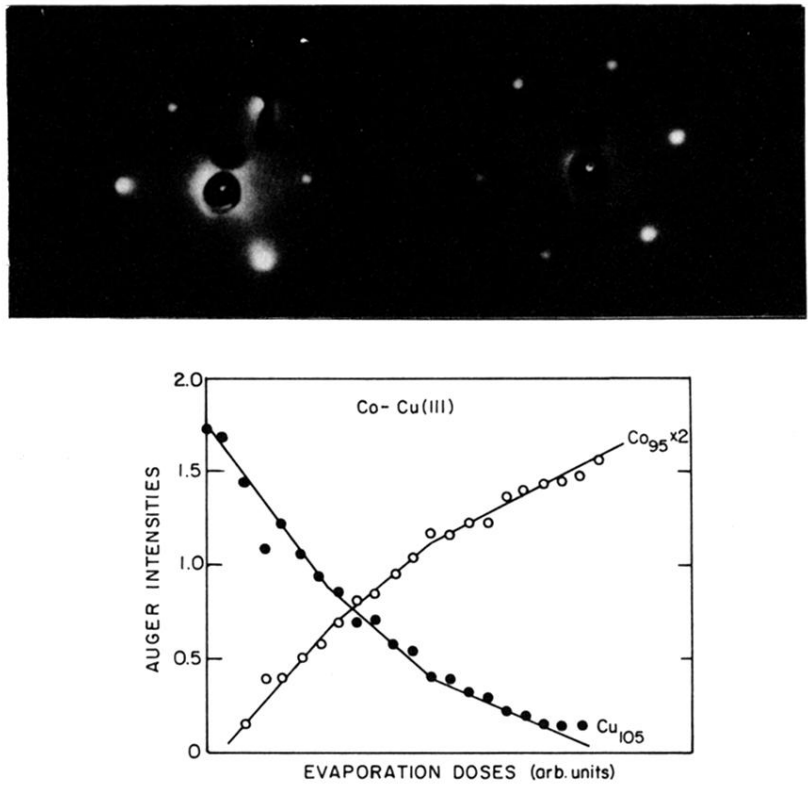

FIG. 2. Peak-to-peak intensities of Cu and Co Auger transitions as a function of Co evaporation doses on top of Cu(111) surface. Intensities are referred to clean-Cu 920-eV Auger peak. LEED patterns, in the upper part of the figure, correspond, from left to right, to a clean Cu(111) surface and to one monolayer of cobalt deposited on it.